System-level Reliability Assessment of Power Stage in Fuel Cell Application

Zhou, Dao; Wang, Huai; Blaabjerg, Frede; Kær, Søren Knudsen; Hansen, Daniel Blom

Published in:
Proceedings of the 2016 IEEE Energy Conversion Congress and Exposition (ECCE)

DOI (link to publication from Publisher):
10.1109/ECCE.2016.7855492

Publication date:
2016

System-level Reliability Assessment of Power Stage in Fuel Cell Application

Dao Zhou[1], Huai Wang[1], Frede Blaabjerg[1], Søren Kundsen Kær[1], Daniel Blom-Hansen[2]

[1] Department of Energy Technology
Aalborg University, Aalborg, Denmark
{zda, hwa, fbl, skk}@et.aau.dk

[2] Dantherm Power A/S
Hobro, Denmark
dbh@dantherm.com

***Abstract* — High efficient and less pollutant fuel cell stacks are emerging and strong candidates of the power solution used for mobile base stations. In the application of the backup power, the availability and reliability hold the highest priority. This paper considers the reliability metrics from the component-level to the system-level for the power stage used in a fuel cell application. It starts with an estimation of the annual accumulated damage for the key power electronic components according to the real mission profile of the fuel cell system. Then, considering the parameter variations in both the lifetime model and the stress levels, the Weibull distribution of the power semiconductors lifetime can be obtained by using Monte Carlo analysis. Afterwards, the reliability block diagram can further be adopted to evaluate the reliability of the power stage based on the estimated power semiconductor reliability. In a case study of a 5 kW fuel cell power stage, the parameter variations of the lifetime model prove that the exponential factor of the junction temperature fluctuation is the most sensitive parameter. Besides, if a 5-out-of-6 redundancy is used, it is concluded both the B_{10} and the B_1 system-level lifetime can be remarkably increased compared to when no redundancy is used.**

I. INTRODUCTION

Fuel cell systems have progressed from being a potential promising technology to a commercially viable power solution for mobile base stations, due to their high energy, high reliability, and less pollution [1], [2]. As a telecom system is possibly connected to a remote power grid location, frequent interruptions lead the availability and reliability of the backup power system of intense importance. Otherwise, the telecom communication lines and systems may suffer from the disruptions and failure.

As shown in Fig. 1, regardless of the stressor types and failure mechanisms, the component failure occurs at the presence of overlap between the stress and strength distribution [3]. Considering a constant stress and strength, a fixed time-to-failure can be expected due to the annually accumulated stress and the degraded strength [4]-[9]. In reality, there are parameters variations in the applied components and the corresponding lifetime models, and a certain degree of uncertainties in the environmental and operation conditions. Therefore, the time-to-failure of individual components is distributed within a certain range. The parameterized distribution for the reliability data set can then be used to estimate the essential life characteristics of the product, such as the reliability or the probability of failure within a specific time, and the failure rate. In the case of the stress and strength distribution, the numerical results can be obtained by using Monte Carlo analysis, a broad class of computational algorithms that rely on repeated random samplings [3]. Afterwards, the parameters of Weibull distribution can be estimated by means of curve fitting, which it is a widely used statistical distribution to represent large samples of life data [10]. By using the reliability block diagram [11], [12], a fault-tree analysis [13], or the Markov chains [14], the system-level reliability metrics can be derived from the component-level, where the estimated lifetime can be compared between the component and system. Meanwhile, the impact of redundancy design on system-level reliability can also be evaluated.

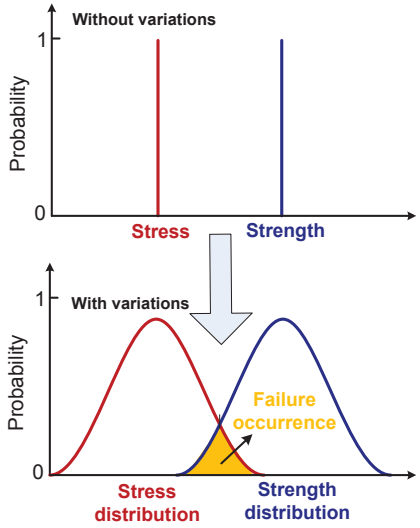

Fig. 1. Stress and strength curve without and with variations.

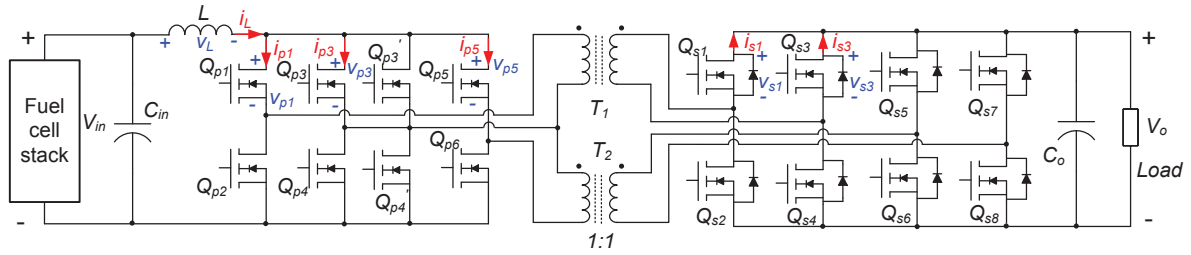

Fig. 2. Dc/dc power converter used in fuel cell system with secondary-side synchronous rectification.

This paper introduces an approach to assess the system-level reliability of the power stage used in a fuel cell application. In section II, with the identified critical components and their main stressor, the annual accumulated damage of the component can be estimated based on the real mission profile. Then, section III focuses on the lifetime distribution from the accumulated damage considering parameter variations of the stress evaluation and the lifetime model. The system-level reliability metrics are then assessed in section IV by using the reliability block diagram. Finally, the concluding remarks are drawn in section V.

II. Annual Accumulated Damage of Key Power Electronic Components without Parameter Variation

As the power semiconductor is one of the most fragile parts of power electronic converters [4], this section starts with the annual damage estimation of the power devices used in a fuel cell backup power system. The topology and the operation principle of the power stage are firstly described, and the key power electronic components should be identified. Afterwards, the procedure of lifetime estimation is addressed based on the stress analysis and lifetime models of power semiconductors. According to the real mission profile, the lifetime expectancy of each power component can be predicted in the case study of a 5 kW fuel cell system.

A. Description of fuel cell power converter

For the backup power application, due to the variable output voltage of the fuel cell stack, a dc/dc power converter is required in order to match the regulated voltage needed in telecom application. The topology with galvanic isolation is shown in Fig. 2, where the specification and main parameters are listed in Table I. It is noted that the rated power of the converter is 1 kW, and six converters are connected in parallel for a 5 kW power stage for the sake of the redundancy. Moreover, synchronous rectification is adopted to achieve lower conduction losses in the situation of the low-voltage and high-current in the secondary-side of the transformer [15].

As shown in Fig. 2, since the reflected voltage of the transformer primary-side can be higher or lower than the fuel cell output voltage, the power converter is able to operate in both step-up mode and step-down mode. In the case of step-up mode, the primary-side inductor is charged by the activation of all transistors, while it is discharged by the parallel connection of the two transformers. It can be seen

Table I
Power Converter Specification and Parameters

Input voltage V_{in}	30 – 65 V
Output voltage V_o	48 V
Maximum output power P_o	1000 W
Primary-side MOSFETs	100 V/74 A, ×8
Secondary-side MOSFETs	100 V/74 A, ×8
Input inductor L	15 μH
Transformer ratio n	1:1
Switching frequency f_{sw}	50 kHz

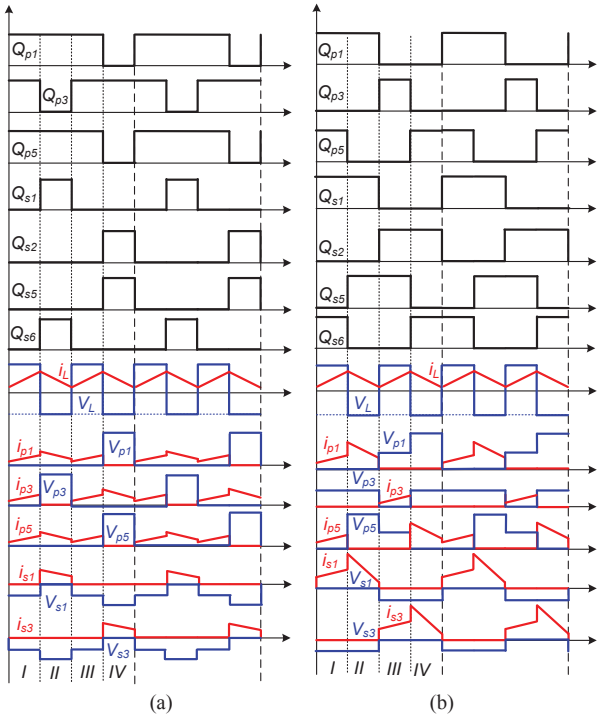

Fig. 3. Key waveforms in dc/dc power converter, where I and V indicate the current and voltage stress of the MOSFET. (a) Step-up mode (1 kW); (b) Step-down mode (250 W).

that during the discharge period, the middle leg carries two times of current of the side legs. As a result, two transistors are selected in parallel in the middle leg for the same current loading of all primary-side transistors. In the case of the step-down mode, the inductor is charged by the parallel

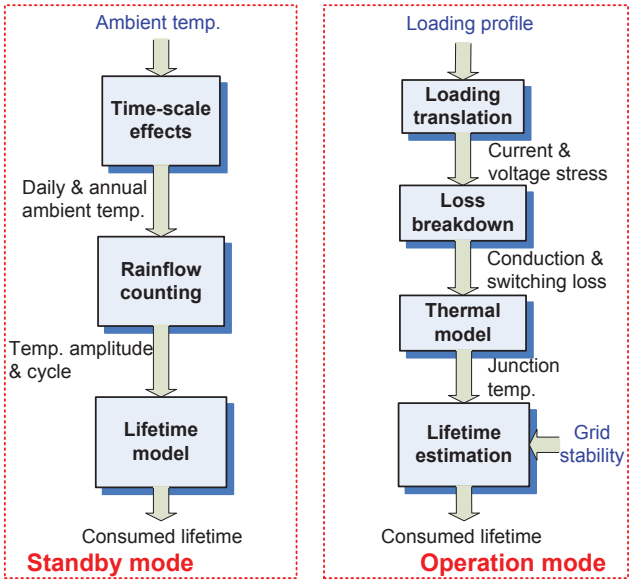

Fig. 4. A flowchart to predict lifetime of power semiconductor used in fuel cell backup power system.

connection of the transformers, while it is discharged by the series connection of the transformers.

At the primary-side, due to the symmetrical loading of the upper and lower transistors, only Q_{p1}, Q_{p3} and Q_{p5} are chosen. Similarly, apart from the symmetrical loading of the upper and lower transistors, the two rectifiers share the same current and voltage loading. As a result, Q_{s1} is able to represent the loading at the secondary-side. Their driving signals as well as the current and voltage stress are illustrated in Fig. 3 in terms of the step-up mode and the step-down mode. It is evident that the performances of the primary-side transistors behave the same as in the step-up mode, but the current and the voltage of the primary-side transistors are unevenly distributed in the step-down mode.

B. Procedure to estimate lifetime of power semiconductor

As aforementioned, the power semiconductor reaches the end-of-lifetime when the overlap occurs between its stress and strength. From the power cycling perspective, the stress analysis is related to the mission profile (e.g. the ambient temperature, the loading profile, and also the grid availability), while the strength model is determined by the selection of the power device. For the backup power application, two major working modes can be defined – the standby mode and the operation mode as shown in Fig. 4.

In the case of the normal grid condition, the fuel cell power converter works in the standby mode. As the power semiconductor stays in idle mode, its junction temperature can be assumed to be the same with the ambient temperature. The daily and the annual ambient temperature can then be classified in order to take the time-scale effect into account. Afterwards, the Rainflow counting is adopted to extract the temperature amplitude and its cycling from the irregular temperature profiles [16]. On the basis of the lifetime model

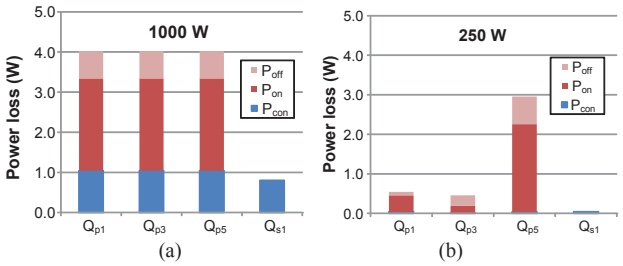

Fig. 5. Loss breakdown of each power semiconductor in the dc/dc converter. (a) Step-up mode (1 kW); (b) Step-down mode (250 W).

of the power semiconductors, the annual consumed lifetime can be calculated.

In the case of a grid outage, the fuel cell stack takes over, and the power converter shifts to work in the operation mode. The junction temperature of the power semiconductor is determined by the ambient temperature and the loading profile. As discussed in [17], 10 hours of full load and 2 hours of 25% load are repeated every half day in the telecom application. These two typical operation points need to be translated into the current and voltage stress of the power semiconductors. According to the loss model and the thermal model of the power device, the junction temperature at various loads can be calculated. With the information of the annual grid outage frequency and its duration, the consumed lifetime can be estimated based on the lifetime model of the power semiconductors.

C. Annnual accumulated damage of power devices

Due to the increased junction temperature caused by the operational loading compared to the ambient temperature, the operation mode dominates the lifetime consumption of the fuel cell power converter [18]. As mentioned before, only Q_{p1}, Q_{p3}, Q_{p5} and Q_{s1} are studied because of the symmetrical feature of the circuit.

The MOSFET losses mainly consist of the conduction loss (P_{con}) and the switching loss, where the switching loss can be further divided into the turn-on losses (P_{on}) and the turn-off losses (P_{off}). According to the loss calculation mentioned in [19], the loss breakdown of the MOSFETs is shown in Fig. 5, where the full load and the quarter load are investigated. It is obvious that in the case of full load, three legs at the primary-side share the same loss distribution. However, the loss distribution becomes uneven in the situation of the 25% load due to the different current and voltage stress among the three legs at the primary-side. Moreover, as the synchronous rectification performs in the way of the natural commutation, there is no switching loss in the secondary-side. Furthermore, it can be seen that the switching losses are much higher than the conduction losses.

Neglecting the thermal coupling from the adjacent devices, each MOSFET can be regarded as an independent thermal system due to its package. Considering the ambient temperature of 40 ºC as the worst case scenario, the mean junction temperature (T_{jm}) and the junction temperature fluctuation (dT_j) can be calculated as shown in Fig. 6, based

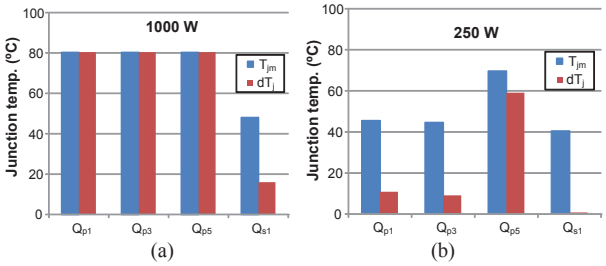

Fig. 6. Thermal profile of each power semiconductor. (a) Step-up mode (1 kW); (b) Step-down mode (250 W).

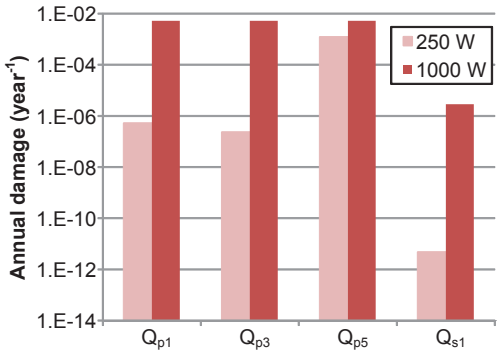

Fig. 7. Annual accumulated damage of the analyzed MOSFETs under 25% load and full load.

on the thermal impedance from the junction to the ambient. It can be seen that the thermal stress of the power semiconductor is proportional to its loss dissipation.

By using the Bayerer lifetime model [20], the cycle to failure N_f can be expressed as,

$$N_f = A \cdot dT_j^{\beta_1} \cdot \exp\left(\frac{\beta_2}{T_{jm}+273}\right) \cdot t_{on}^{\beta_3} \quad (1)$$

where the power cycle is closely related to the junction temperature swing dT_j, the mean junction temperature T_{jm} as well as its on-time duration t_{on}. Besides, A, β_1, β_2, and β_3 can be obtained according to test data provided by the manufacturer of the device.

In the case of the severe working condition, the outage of the power grid may occur daily, and the outage duration lasts 4 hours in average. Together with the thermal profile described in Fig. 6, the cycle to failure can be calculated in the conditions of the full load and the quarter load, respectively. On the other hand, the annual power cycling of each loading condition can be estimated with the grid outage duration. On the basis of the Miner's rule [21], the annual damage D can be calculated by annual power cycling n over the corresponding end-of-life power cycles,

$$D = \sum \frac{n_{(i)}}{N_{f(i)}} \quad (2)$$

where subscript i indicates different loading conditions like full load and 25% load.

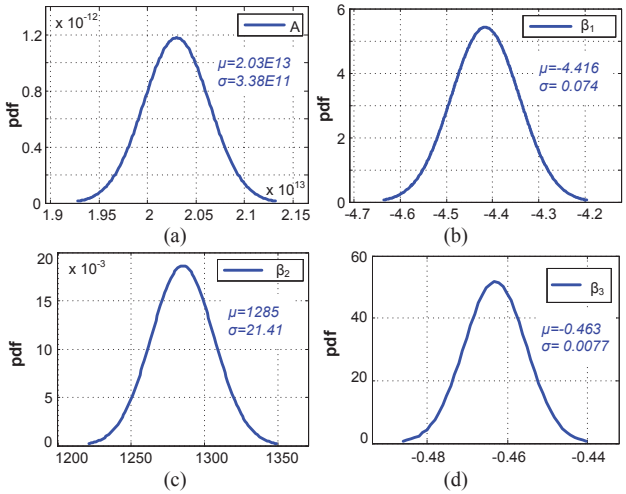

Fig. 8. Normal distrbution of the factors from the strength model. (a) A – scaling factor; (b) β_1 – exponential factor of temperature swing; (c) β_2 – exponential factor of average temperature; (d) β_3 – exponential factor of on-state time.

The annual accumulated damage of the power device under two different loading levels is shown in Fig. 7. It can be seen that Q_{p5} has the highest lifetime consumption of 0.64%, while the Q_{s1} consumes the least due to their remarkably various thermal stress.

III. Time-to-Failure Distribution Considering Parameter Variations

The previous section gives a fixed annual damage of MOSFETs used in power converter, but the uncertainties due to the statistic properties of the applied lifetime model and the parameter variations of the power device should also be taken into account. Therefore, a statistical approach to analyze lifetime performance subject to parameter variations is carried out in detail by means of Monte Carlo simulation. Finally, the time-to-failure distribution of the power semiconductor can be estimated by considering parameter variations.

A. Variations in lifetime model

Since the lifetime model is obtained from the accelerated testing results based on a specific number of testing samples, there is a certain degree of uncertainty of derived constant parameters. As mentioned in [20], the coefficients of the Bayerer model are fitted by a large number of test data, and they are given within a certainty range.

All the parameters in the lifetime model are modeled by means of Normal probability density function (pdf), which can be seen in Fig. 8, assuming that A, β_1, β_2 and β_3 experience a variation of 5%. It is noted that μ denotes the mean value of the distribution, and σ denotes the standard deviation. In order to simplify the thermal stress from both the full load and the quarter load, the equivalent static values of the lifetime data can be calculated in Table II. Since the number of thermal cycles is related to the grid outage frequency, the equivalent number of cycles to failure can be

Table II
EQUIVALENT STATIC VALUE FOR EACH MOSFET

	Q_{p1}	Q_{p3}	Q_{p5}	Q_{s1}
Number of cycles per year n	365	365	365	365
Annual damage D	5.20E-2	5.20E-2	6.30E-2	2.87E-6
Number of cycles to failure N_f	7.02E4	7.02E4	5.79E4	1.27E8
Mean junction temperature T_{jm}	62.5	61.0	102.7	43.3
On-state time t_{on}	14400	14400	14400	14400
Junction temperature fluctuation dT_j	83.9	85.5	54.4	14.4

calculated together with the annual damage. Afterwards, as the mean junction temperature is determined by the thermal profile as well as the probabilities of the loading condition, the equivalent static junction temperature fluctuation can be calculated together with the on-state time, which is the same as the period of the grid outage.

In order to evaluate the effects of parameter variations on the annual damage of the MOSFETs, a sensitivity analysis is performed by considering each individual parameter variations, while other parameters are maintained to the mean value of their distributions. Each distribution is sampled by using Monte Carlo simulations, whose sample numbers results in the accuracy of the output distribution. As a consequence, 10,000 samplings are chosen to establish the accumulated damage distribution.

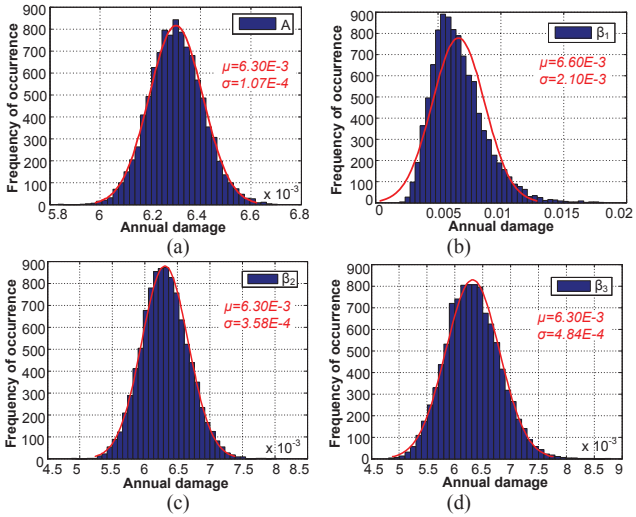

Fig. 9. Annual damage distribution considering the parameter variations in the lifetime model. (a) A – scaling factor; (b) β_1 – exponential factor of temperature swing; (c) β_2 – exponential factor of average temperature; (d) β_3 – exponential factor of on-state time.

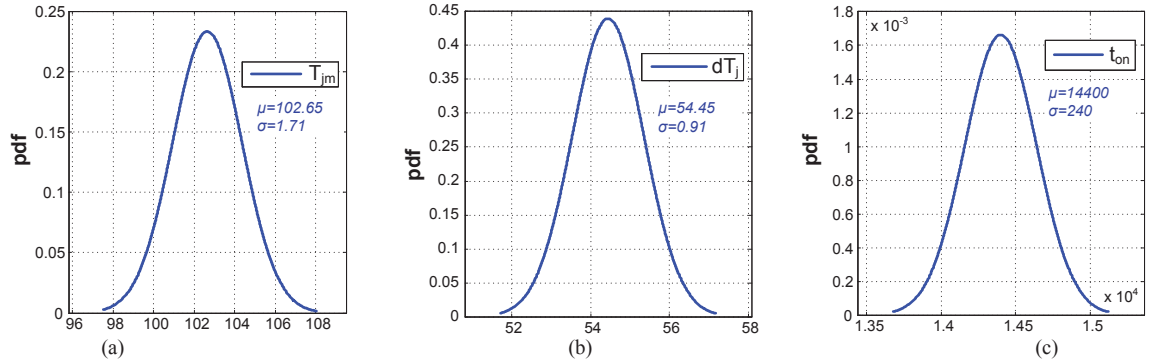

Fig. 10. Parameter varations by Normal distribution from stress evaluation. (a) T_{jm} – average junction temperature; (b) dT_j – junction temperature swing; (c) t_{on} – on-state duration.

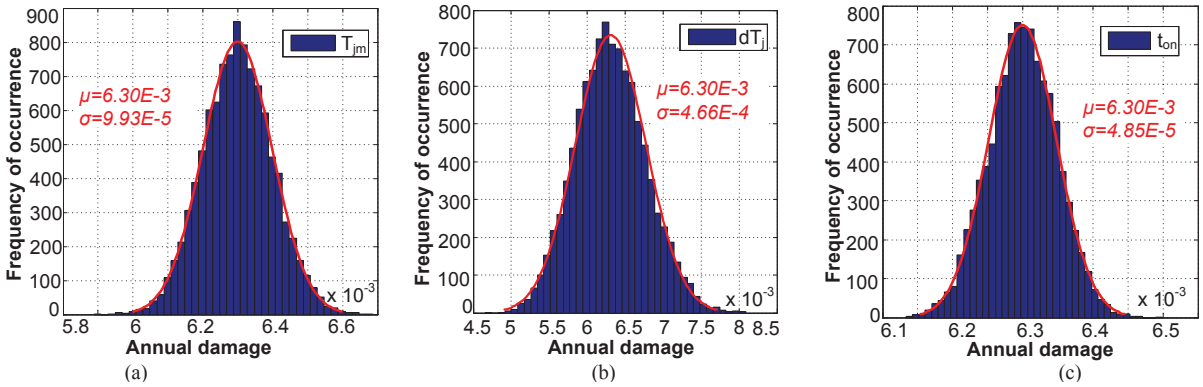

Fig. 11. Annual damage distribution considering variations in stress. (a) T_{jm} – average junction temperature; (b) dT_j – junction temperature swing; (c) t_{on} – on-state duration.

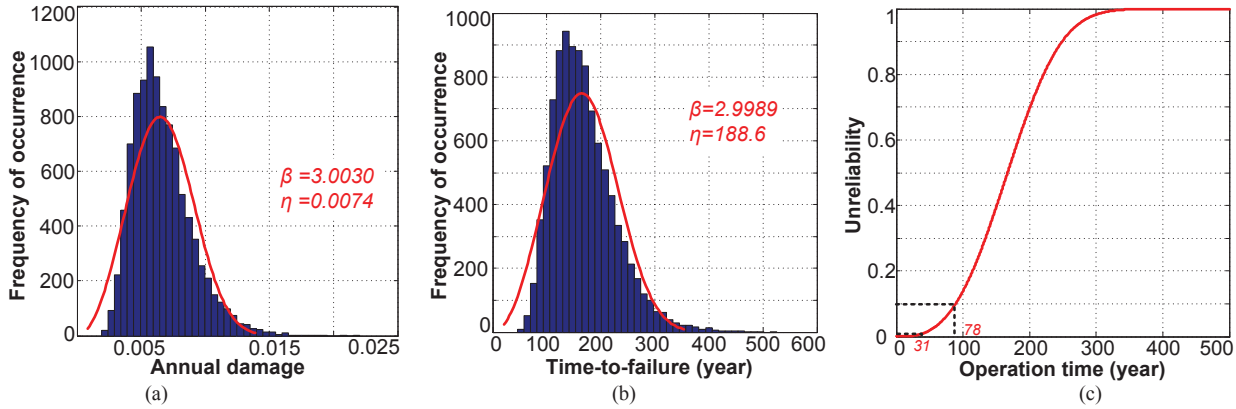

Fig. 12. Monte Carlo analysis considering all parameter variations from the stress evaluation and lifetime model. (a) Annual damage; (b) Time-to-failure distribution; (c) Accumulated percentage of failure (i.e. unreliability) along with the operation time.

Considering the four parameter variations of the applied lifetime mode, the annual damage distribution of the most stressed power semiconductor Q_{p5} is shown in Fig. 9. The blue pillars indicate the frequency of occurrence, while the red curve is the fitting pdf of the normal distribution. It is noted that the annual damage deviates most in the case of the exponential factor of the junction temperature fluctuation β_1, which indicates that the lifetime model is most sensitive to this factor.

B. *Variations in stress*

The second type of the uncertainty exists due to variances in the manufacturing process (like the typical, maximum and minimum on-state resistance of the MOSFET), which results in the variation of the mean junction temperature and the junction temperature fluctuation. Meanwhile, the duration of the grid outage is randomly distributed because of the various working locations.

For the illustration purpose, the Q_{p5} is selected as an example. The mean junction temperature, junction temperature fluctuation and the on-state time experience a variation of 5% as shown in Fig. 10. Again, by using Monte Carlo simulation, the sensitivity analysis from the stress evaluation can be calculated and seen in Fig. 11. It is noted that the mean annual damage of these variations have the same value of 6.30E-3, which is consistent with the static value.

C. *Time-to-failure distribution by using Weibull*

In the condition that all parameter variations are taken into account, by using Monte Carlo simulation, the annual damage distribution is depicted in Fig. 12(a). It is known the time-to-failure data can typically follow the Weibull distribution,

$$f(t) = \frac{\beta}{\eta}\left(\frac{t}{\eta}\right)^{\beta-1} \cdot \exp\left[-\left(\frac{t}{\eta}\right)^{\beta}\right] \qquad (3)$$

where η denotes the scale parameter, and β denotes the shape parameter.

As a result, the fitting curve can be obtained with the scale parameter of 7.4E-3 and the shape parameter of 3.00.

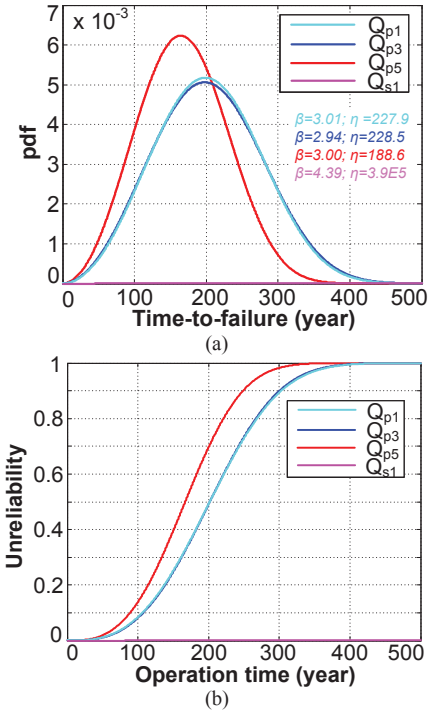

Fig. 13. Monte Carlo analysis of four typical power switches. (a) End-of-life probability density function; (b) Accumulated failure.

Assuming that the mission profile is repeated every year, the probability of the lifetime is distributed as shown in Fig. 12(b). Afterwards, the unreliability or failure of the power switch Q_{p5} can be deduced, which is the integration of the probability density function. It is noted that 10% and 1% of MOSFETs are predicted to have a failure after 78 and 31 years of operation.

IV. SYTEM-LEVEL REALIBITY METRICS BY USING RELIABILITY BLOCK DIAGRAM

In this section, similar Monte Carlo analysis is extended to the key components of the power electronics converter, and

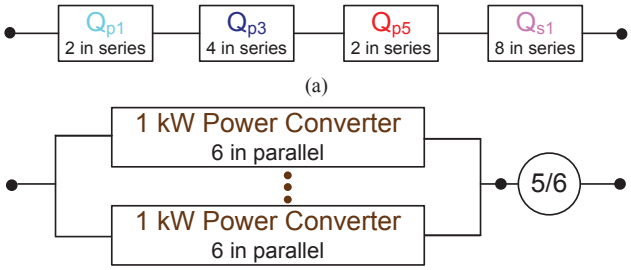

Fig. 14. Reliability metrics by using reliability block diagram. (a) Composition of 1 kW power converter; (b) Composition of 5 kW power stage.

their lifetime distribution can be obtained. Afterwards, the system-level reliability is assessed by using the reliability block diagram, where the redundancy of the paralleled power converters is taken into account as well.

A. Time-to-failure distribution of key components

With the static equivalent values of each component as listed in Table II, the lifetime distribution of the key MOSFETs is shown in Fig. 13(a), considering the 5% parameter variations from the lifetime model and the stress analysis. Since the scale parameter of the Weibull function denotes the value when 63.2% failure occurs, it is predicted that the Q_{p5} has the lowest scale parameter according to the accumulated damage estimation as shown in Fig. 7. In fact, it can be seen that Q_{p5} has the lowest scale parameter of 189.

For the accumulated failure as shown in Fig. 13(b), it can be seen that Q_{p1}, Q_{p3} and Q_{p5} reach end-of-life at the operation time around 500 operation years. However, 500-year operation hardly contributes on the lifetime consumption of Q_{s1} due to its remarkably higher scale parameter of 3.9E5.

B. System-level reliability metrics

In order to assess the reliability metrics of the whole power stage in the fuel cell system, major steps can be divided into the reliability analysis of a 1 kW power converter and a 5 kW power stage, respectively. By using the reliability block diagram, the procedure to calculate the reliability metrics is shown in Fig. 14. It can be noted that due to the same time-to-failure characteristic of the representing power devices, only these components are depicted.

For the reliability analysis of 1 kW power converter (sub-system), the existence of any failed MOSFET (component) results in the abnormal operation of the power converter, which indicates that all MOSFETs are connected in series in the reliability block diagram. As the reliability of the series block is the product of the all components, the failure function of the sub-system F_{sub} can be expressed by the component failure function F_{com} [3], [11],

$$F_{Sub}(\mathrm{t}) = 1 - \prod_{i} (1 - \mathrm{F}_{Com(i)}(\mathrm{t})) \tag{4}$$

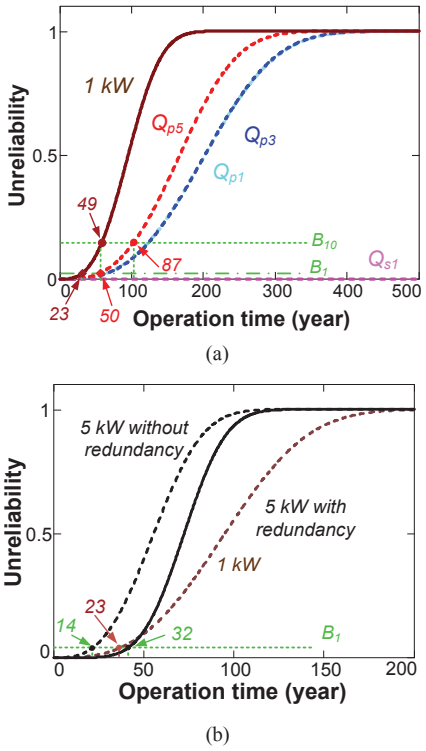

Fig. 15. Accumulated percentage of failure. (a) From MOSFETs (component) to power converter (sub-system); (b) From power converter (sub-system) to power stage (system).

As mentioned before, the MOSFETs are not evenly stressed and the four representing MOSFETs can be found. The reliability of 1 kW power converter can then be calculated by considering all the MOSFETs used in the primary-side and secondary-side.

As shown in Fig. 15(a), the sub-system reliability can be deduced from the component-level reliability. It can be seen that the failure percentage of the sub-system reaches 100% after around 150 operation years, much lower than the component lifetime. Moreover, the B_{10} lifetime of the most stressed component Q_{p5} is 87 years, while the B_{10} lifetime of the 1 kW power converter is reduced to 49 years. Besides, the more critical B_1 lifetime of the most stressed component and the power converter are 50 years and 23 years, respectively.

For the reliability analysis of the whole power stage, it can be estimated from the reliability analysis of the 1 kW power converter, where six 1 kW power converter are connected in parallel for the 5 kW application. In the case of *m*-out-of-*n* redundancy, the failure function of the system F_{sys} can be expressed as [3],

$$F_{Sys}(\mathrm{t}) = \sum_{i=0}^{m-1} \frac{n!}{i!(\mathrm{n}-\mathrm{i})!} \cdot (1 - \mathrm{F}_{Sub}(\mathrm{t}))^{i} \cdot \mathrm{F}_{Sub}(\mathrm{t})^{n-i} \tag{5}$$

The failure function of the whole power stage is shown in Fig. 15(b), where the cases with and without redundancy are compared as well. Due to the fact that 5 reliability blocks are series connected in the condition of without redundancy, the lifetime of the power stage is significantly reduced compared to the 1 kW power converter. However, in the case of using redundancy, the reliability of the power stage can be enhanced compared with no redundancy. For instance, it can be seen that the B_1 lifetime of 1 kW power converter is 23 year. At the same time, the expected operation time of the power stage without redundancy is 14 years, while the expected lifetime with redundancy can be enhanced to 32 years.

V. CONCLUSION

This paper has described an approach to convert the component-level reliability to system-level reliability in the application of a fuel cell power converter. Based on the real mission profile fuel cell system, a fixed lifetime of each power semiconductor can be estimated. By means of Monte Carlo analysis, the lifetime distribution can be obtained by considering the parameter variations from both the stress analysis and lifetime model. With the help of a reliability block diagram, the reliability of the component can be extended to the system. The lifetime distribution has an advanced estimation of important life characteristics, such as reliability or probability of failure at a specific time, and failure rate. In a case study of 5 kW fuel cell system, the parameter variations of the lifetime model prove that the exponential factor from the junction temperature fluctuation is the most sensitive. Besides, if a 5-out-of-6 redundancy strategy is used for six paralleled power converters, it is concluded the B_1 system-level lifetime is increased from 14 years to 32 years. It guides a design tradeoff between the manufacturer cost and reliability consideration when using the redundant topology.

REFERENCES

[1] K. Rajashekara, "Hybrid fuel-cell strategies for clean power generation," *IEEE Trans. on Industry Applications*, vol. 41, no. 3, pp. 682-689, May 2005.

[2] H. Tao, J. L. Duarte, and M. A. M. Hendrix, "Line-interactive UPS using a fuel cell as the primary source," *IEEE Trans. on Industrial Electronics*, vol. 55, no. 8, pp. 3012-3021, Aug. 2008.

[3] P. D. T. O'Connor, and A. Kleyner, *Practical Reliability Engineering (fifth edition)*. New York, USA: Wiley, 2012.

[4] H. S. Chung, H. Wang, F. Blaabjerg, and M. Pecht, *Reliability of power electronic converter systems*. IET Publisher, 2015.

[5] H. Wang, M. Liserre, F. Blaabjerg, P. de P. Rimmen, J. B. Jacobsen, T Kvisgaard, and J. Landkildehus, "Transitioning to physics-of-failure as a reliability driver in power electronics," *IEEE Journal of Emerging and Selected Topics in Power Electronics*, vol. 2, no. 1, pp. 97-114, Mar. 2014.

[6] K. Ma, M. Liserre, F. Blaabjerg, and T. Kerekes, "Thermal loading and lifetime estimation for power device considering mission profiles in wind power converter," *IEEE Trans. on Power Electronics*, vol. 30, no. 2, pp. 590-602, Feb. 2015.

[7] Y. Yang, H. Wang, F. Blaabjerg, and K. Ma, "Mission profile based multi-disciplinary analysis of power modules in single-phase transformerless photovoltaic inverters," *in Proc. of EPE 2013*, pp.1-10, 2013.

[8] D. Zhou, F. Blaabjerg, M. Lau, and M. Tonnes, "Optimized reactive power flow of DFIG power converters for better reliability performance considering grid codes," *IEEE Trans. on Industrial Electronics*, vol. 62, no. 3, pp. 1552-1562, Mar. 2015.

[9] P. D. Reigosa, H. Wang, Y. Yang, and F. Blaabjerg, "Prediction of bond wire fatigue of IGBTs in a PV Inverter under a long-term operation," *IEEE Trans. on Power Electronics*, vol. 31, no. 10, pp. 7171-7182, Oct. 2016.

[10] ReliaSoft Corporation, "Life data analysis reference," [Online]. http://reliawiki.org/index.php/Life_Data_Analysis_Reference_Book, 2015.

[11] X. Yu, and A. M. Khambadkone, "Reliability analysis and cost optimization of parallel-inverter system," *IEEE Trans. on Industrial Electronics*, vol. 59, no. 10, pp. 3881-3889, Oct. 2012.

[12] F. Richardeau, and T. T. L. Pham, "Reliability calculation of multilevel converters: theory and applications," *IEEE Trans. on Industrial Electronics*, vol. 60, no. 10, pp. 4225-4233, Oct. 2013.

[13] L. Placca, and R.Kouta. "Fault tree analysis for PEM fuel cell degradation process modelling." *International Journal of Hydrogen Energy*, vol. 36, no. 19, pp. 12393-12405, 2011.

[14] A. Khosroshahi, M. Abapour, and M. Sabahi, "Reliability evaluation of conventional and interleaved DC–DC boost converters," *IEEE Trans. on Power Electronics*, vol. 30, no. 10, pp. 5821-5828, Oct. 2015.

[15] W. Feng, F. C. Lee, P. Mattavelli, and D. Huang, "A universal adaptive driving scheme for synchronous rectification in LLC resonant converters," *IEEE Trans. on Power Electronics*, vol. 27, no. 8, pp. 3775-3781, Aug. 2012.

[16] M. Matsuishi, and T. Endo, "Fatigue of metals subjected to varying stress", *Japan Soc. Mech. Engineering*, 1968.

[17] M. J. Vasallo, J. M. Andujar, C. Garcia, and J. J. Brey, "A methodology for sizing backup fuel-cell/battery hybrid power systems," *IEEE Trans. on Industrial Electronics*, vol. 57, no. 6, pp. 1964-1975, Jun. 2010.

[18] D. Zhou, H. Wang, F. Blaabjerg, S. K. Kaer, and D. B. Hansen, "Real mission profile based lifetime estimation of fuel-cell power converter," *in Proc. of IPEMC 2016*, pp. 1-8, 2016.

[19] Infineon, "MOSFET power losses calculation using the datasheet parameters," [Online]. http://application-notes.digchip.com/070/70-41484.pdf

[20] R. Bayerer, T. Herrmann, T. Licht, J. Lutz, and M. Feller, "Model for power cycling lifetime of IGBT modules - various factors influencing lifetime," *in Proc. of Integrated Power Systems (CIPS) 2008*, pp.1-6, 2008.

[21] H. C. Yildirim, G. Marquis, and Z. Barsoum, " Fatigue assessment of high frequency mechanical impact (HFMI)-improved fillet welds by local approaches," *International Journal of Fatigue*, vol. 52, pp. 57–67, 2013.